PAPER

A eutectic-alloy-infused soft actuator with sensing, tunable degrees of freedom, and stiffness properties

View the article online for updates and enhancements.

A eutectic-alloy-infused soft actuator with sensing, tunable degrees of freedom, and stiffness properties

Yufei Hao, Tianmiao Wang, Zhexin Xie, Wenguang Sun, Zemin Liu, Xi Fang, Minxuan Yang and Li Wen

School of Mechanical Engineering and Automation, Beihang University, Beijing 100191, People's Republic of China

E-mail: liwen@buaa.edu.cn

Abstract

This paper presents a soft actuator embedded with two types of eutectic alloys which enable sensing, tunable mechanical degrees of freedom (DOF), and variable stiffness properties. To modulate the stiffness of the actuator, we embedded a low melting point alloy (LMPA) in the bottom portion of the soft actuator. Different sections of the LMPA could be selectively melted by the Ni–Cr wires twined underneath. To acquire the curvature information, EGaIn (eutectic gallium indium) was infused into a microchannel surrounding the chambers of the soft actuator. Systematic experiments were performed to characterize the stiffness, tunable DOF, and sensing the bending curvature. We found that the average bending force and elasticity modulus could be increased about 35 and 4000 times, respectively, with the LMPA in a solid state. The entire LMPA could be melted from a solid to a liquid state within 12 s. In particular, up to six different motion patterns could be achieved under each pneumatic pressure of the soft actuator. Furthermore, the kinematics of the actuator under different motion patterns could be obtained by a mathematical model whose input was provided by the EGaIn sensor. For demonstration purposes, a two-fingered gripper was fabricated to grasp various objects by adjusting the DOF and mechanical stiffness.

Keywords: variable stiffness, tunable degrees of freedoms, soft sensing, multi-functionality

S Supplementary material for this article is available online

(Some figures may appear in colour only in the online journal)

1. Introduction

Soft robots have been utilized for a variety of purposes such as manipulation [1], bioinspired robots [2, 3], wearable devices [4], and minimally invasive surgery [5], etc, because of their inherent compliance, easy-to-fabricate, and safely interacting with the environments. Until now, some drawbacks of soft robots still exist. For example, the commonly used soft materials such as silicone elastomer have a relatively low mechanical stiffness which restricts the load capacity of the soft robots. In addition, most soft actuators can only actuate with one motion pattern, which limits their flexibility and adaptability. Soft robots' large deformation also

poses challenges for obtaining the sensory feedback for the bending curvature, position, etc. To enable the soft robots with multi-functionality, researchers have begun to put efforts on the variable stiffness, programmable degrees of freedoms, and sensing capabilities of soft robots.

Recent work on variable stiffness can be divided into two categories: that based on actuation-based mechanisms and that on materials with variable stiffness. The actuation-based mechanism is achieved by changing the inner pressure of a sealed structure. That is, by increasing the inner pressure, the stiffness of the pneumatic actuators will increase [6, 7]. Alternatively, by vacuuming a membrane packed with many particles, the granular material contracts and hardens, thus
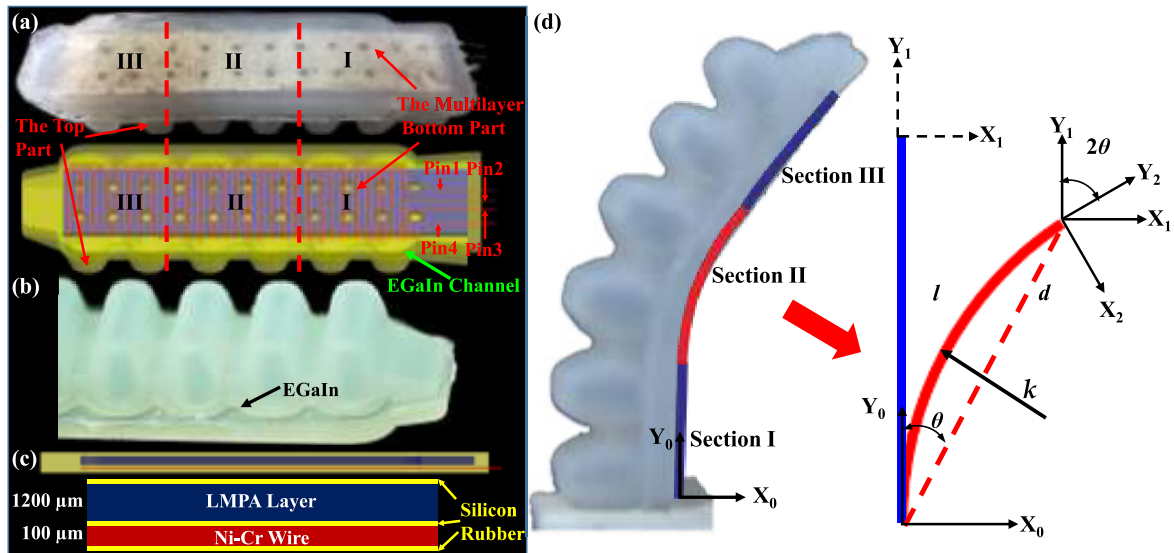
Figure 1. The design and mathematical model of the actuator. (a) The actuator consists of a top ribbed portion and a multilayer bottom portion. EGaIn is injected into the microchannel of the top to measure the curvature. Furthermore, the LMPA's three sections (I–III) could be separately melted by applying electrical currents to any two of the four pins. Thus, the actuator has six motion patterns. Pattern 1: all the sections are melted by applying current to pins 1 and 2. Pattern 2: sections I and II are melted by applying current to pins 2 and 4. Pattern 3: section I is melted by applying current to pins 2 and 3. Pattern 4: sections II and III are melted by applying current to pins 1 and 3. Pattern 5: section II is melted by applying current to pins 3 and 4. Pattern 6: section III is melted by applying current to pins 1 and 4. (b) The details of the EGaIn sensor. (c) The details of the multilayer bottom portion. This part has three distinct layers: the LMPA, the Ni–Cr wire, and the silicon rubber. (d) The mathematical model to describe the variable DOF of the actuator.

the structure will be stiffer [8, 9]. As for variable stiffness materials, rigidity can be changed by applying magnetic [10], electrical [11], or thermal stimuli [12]. The stiffness of shape memory polymers (SMPs) can be changed when heated above the glass transition temperature [13, 14]. Shape memory alloy (SMA) can also change the stiffness by applying heat [15].

Recent progress on changing the DOF of soft robots includes mechanical methods and the integration of multi-materials. The mechanical method is often achieved by increasing the pressure in serial or parallel pneumatic/fluidic channels that can be separately pressurized [16, 17]. The multi-materials prototypes, such as the fiber-reinforced actuator, can perform varied motions by changing the angle of the fibers during the design stage [18]. Furthermore, studies also accomplish similar tasks by using paper [19], sleeves [20], or fabric patches [21] in tandem with soft actuators. A few other studies have attempted to adjust motion patterns in operation by heating shape memory polymers [21] or activating conductive elastomers [23] located in certain areas of soft robots.

The low-melting-point alloys (LMPAs), which are eutectic alloys with very low melting points (47 °C–138 °C), can alter its stiffness over a wide range and can self-heal from the broken state caused by the external impact. The stiffness range of LMPAs, when they transform from a solid state to liquid state, can be several magnitudes greater than that achieved with other materials [24]. After an impact, their mechanical properties can be recovered via a reheating-recrystallizing cycle [25]. Recently, some studies have begun incorporating LMPAs into soft robots for adjusting stiffness, including the continuum manipulator [26], the metal and elastomer foam [25], and the variable stiffness fiber [27].

However, few studies have implemented a robotic device that allows DOF and stiffness to be changed simultaneously by using LMPAs. The EGaIn sensing has been investigated extensively in recent studies [28–32]. Little work, however, has incorporated EGaIn into a variable stiffness/DOF device for curvature sensing.

In this study, we present a soft actuator integrated with sensing, variable stiffness, and tunable DOF properties using eutectic alloys. The soft actuator was infused with two types of eutectic alloys: the LMPA for the variable stiffness/DOF and EGaIn for sensing. To change the stiffness of the actuator, we used Ni–Cr wires to melt the LMPA layer embedded in the bottom portion. Furthermore, different sections of the LMPA layer could be selectively melted by applying a current to different pins of the Ni–Cr wire, thus changing the DOF of the actuator. Apart from LMPAs, we inject EGaIn, the other eutectic alloy with a low melting point (15.6 °C), into the microchannels underneath the air chamber of the actuator for curvature feedback. Systematic experiments were conducted to test the thermal behavior, mechanical properties, tunable DOF, and sensing property of the actuator. Furthermore, a two-finger gripper infused with eutectic alloys was fabricated for gripping objects of different sizes and shapes.

2. Materials and methods

2.1. The design of the eutectic-alloy-infused soft actuator

The details of the eutectic-alloy-infused soft actuator are described in figure 1. Referring to figure 1(a), the actuator is composed of a typically ribbed top part and a multilayer bottom

part. The ribbed structure was chosen for its fast response, low-level strain [33] and bi-directional motion properties [34]. To acquire the curvature information, EGaIn (75.5% Ga and 24.5% In by weight) was injected into the microchannel (with the dimension of 400 μm by 400 μm) of the soft actuator. The microchannel was designed to locate at the bottommost portion of the chamber (as shown in figure 1(b)). This structure has the advantage of easy fabrication and can withstand the most strain under actuation. The multilayer bottom part contains three layers (figure 1(c)): (1) the LMPA layer, which could change the stiffness of the actuator under thermal actuation; (2) the Ni–Cr wire, which was used to melt the LMPA; (3) the silicone rubber (Dragon Skin 10, Smooth-on Inc., USA), which was used to separate the wires and LMPA to prevent any unexpected galvanic conduction and seal them in a compact space.

The LMPA used is a eutectic alloy of 32.5% Bi, 51% In, and 16.5% Sn by weight (Roto144F, Rotometals Inc., USA). The material was selected for its low melting point (62 °C) and high stiffness when in a solid state. From figure 1(a), it can be seen that the LMPA layer is a rectangular plate with rows of holes (2 mm diameter). The holes were used to ensure a compact connection between the silicone rubber and the LMPA because the rubber has no adhesive force on the LMPA. To implement the LMPA layer that enable variable stiffness and controllable DoF, we first fabricated the mold with silicon elastomer, then we injected the melted LMPA into the mold. After solidified of the LMPA, the LMPA layer was peeled from the mold. The Ni–Cr wire was twined into shape of 'square wave' and then dipped into a layer of the uncured silicone elastomer (Dragon Skin 10, Smooth-on Inc., USA). Then the LMPA layer, the Ni–Cr wire, as well as the top layer were bonded together by uncured silicone elastomer. To selectively melt the different sections of the LMPA layer (section I–III in figure 1(a)), we added two more pins to the Ni–Cr wire (four pins in total). Applying current to any two of the four pins, the LPMA above the energized wire is melted. Thus the corresponding sections of the actuator can be bent while pressurized. As a result, the actuator will have six motion patterns under the same pressure. The relationships between the motion patterns and the pins are described in the caption of figure 1.

2.2. The mathematical model of the soft actuator with tunable DOF

Compared to most soft actuators, which typically have only one motion pattern, the actuator with embedded LMPA attains more motion patterns by softening its different sections. A mathematical model was established to describe the kinematics of the actuator under the various motion patterns. We hypothesize that the boundaries between the neighboring sections are tangent and focused on the bottom profile of the actuator. As figure 1(d) shows, the bending of one section could be represented by translating the coordinate $X_0 - Y_0$ to $X_1 - Y_1$ with the distance d, then rotating with the angle -2θ to $X_2 - Y_2$.

So the homogeneous transformation matrix from $X_0 - Y_0$ to $X_2 - Y_2$ is:

$$
{}_0^2A = \begin{bmatrix} \cos 2\theta & \sin 2\theta & 0 & d\sin\theta \\ -\sin 2\theta & \cos 2\theta & 0 & d\cos\theta \\ 0 & 0 & 1 & 0 \\ 0 & 0 & 0 & 1 \end{bmatrix}. \tag{1}
$$

According to the geometrical relationships, we could get:

$$
d = \frac{l\sin\theta}{\theta}, \tag{2}
$$

$$
\theta = \frac{kl}{2}, \tag{3}
$$

where l is the length of the actuator and k is the curvature. Substituting equations (2) and (3) into (1), equation (1) could be rewritten as:

$$
{}_0^2A = \begin{bmatrix} \cos kl & \sin kl & 0 & \frac{1-\cos kl}{k} \\ -\sin kl & \cos kl & 0 & \frac{\sin kl}{k} \\ 0 & 0 & 1 & 0 \\ 0 & 0 & 0 & 1 \end{bmatrix}. \tag{4}
$$

If the section is in the solid state, as the blue line shows in figure 1(d), the transformation matrix could be written as:

$$
{}_0^1A = \begin{bmatrix} 1 & 0 & 0 & 0 \\ 0 & 1 & 0 & l \\ 0 & 0 & 1 & 0 \\ 0 & 0 & 0 & 1 \end{bmatrix}. \tag{5}
$$

When $\theta \to 0, k \to 0$, and

$$
\lim_{k \to 0} {}_0^2A = \begin{bmatrix} \cos kl & \sin kl & 0 & \frac{\sin^2 kl/2}{k/2} \\ -\sin kl & \cos kl & 0 & \frac{\sin kl}{k} \\ 0 & 0 & 1 & 0 \\ 0 & 0 & 0 & 1 \end{bmatrix} = \begin{bmatrix} 1 & 0 & 0 & 0 \\ 0 & 1 & 0 & l \\ 0 & 0 & 1 & 0 \\ 0 & 0 & 0 & 1 \end{bmatrix}. \tag{6}
$$

So the solid section could also be represented by ${}_0^2A$. For the three sections, the transformation matrix could be defined as:

$$
{}_0^3T = {}_0^1T_1^2T_2^3T, \tag{7}
$$

where ${}_{i-1}^{i}T$ is the transformation matrix ${}_0^2A$ for the ith section. According to this mathematical model, for each bending DoF, one can obtain the profile of the actuator with the curvature as the input.

To validate the various motion patterns, we fixed the actuator to a base, then powered the matched pins interpreted in figure 1 to melt the corresponding sections. After that, the actuator was inflated to 30 kPa, and the profile of the actuator was captured for later analysis. For application demonstration, we fabricated a gripper by mounting two actuators to a base, then used the gripper to grasp objects in various sizes and shapes. Abandoning the traditional bending-enclosing grasp strategy [35], we first melted the corresponding sections of the actuator based on the geometric features of the objects,
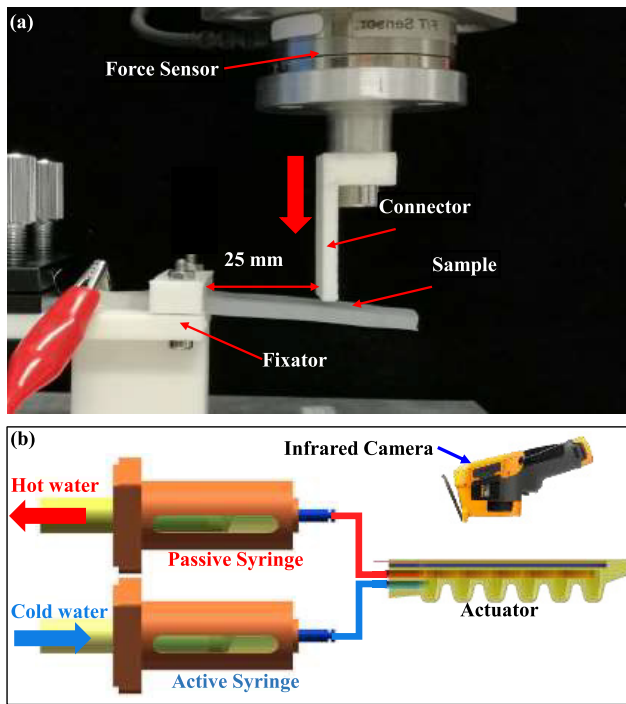
Figure 2. The experimental setups. (a) The setup for the bending force test. The sample was fastened to a fixator. The connector was fixed to a robot arm via the force sensor. The lateral distance between the connector and the base of the sample was 25 mm. (b) The setup for the water cooling experiment. After heating the LMPA, the cold water was pushed into the actuator by the active syringe, while the hot water was pulled out of the actuator via the passive syringe. The infrared camera recorded the temperature change throughout the whole process.

then inflated the actuator to achieve more stable and active-adaptable grasping.

2.3. The mechanical stiffness measurement of the soft actuator

Two experiments (bending strength and tensile strength) were conducted to test the variable stiffness of the actuator and its repeatability. For convenience, only the bottom part was tested because it dominates the stiffness of the entire structure. The experimental setup for the bending test is shown in figure 2(a). The sample was fastened to the fixator. The connector was installed on a robot arm (MOTOMAN MH3F, YASKAWA Inc., Japan) via the force sensor (Mini 40 F/T sensor, ATI, USA). During the test, the robot arm moved vertically downward with the speed of 0.5 mm s^{-1}, driving the connector to push the sample downward. The force along the z-direction was acquired via a LabVIEW program at a sample rate of 20 Hz. After moving 2 mm, the robot arm suspended 5 s then moved again. The total displacement was 20 mm for the whole process. Three samples were provided for this experiment. To verify the repeatability, we tested each sample under three reheating-recrystallizing cycles. To test the bending strength of the sample under the liquid state, the LMPA was melted with a current of 0.4 A and kept soft during the whole process.

The tensile strength was tested via the universal material test machine (exceed model E44, MTS, USA). For this experiment,

the ends of the sample were fixed to the two clamps of the machine; then the upper clamp moved upwards at the speed of 0.5 mm s^{-1}. The force and the strain data were recorded simultaneously at the sample rate of 20 Hz. Three samples were measured for the liquid state and solid state, respectively. Additionally, each sample was tested under three reheating-recrystallizing cycles to verify the repeatability of the mechanical property.

2.4. The thermal conduction behavior test

Two experiments were designed to evaluate the heating performance of the LMPA. For these experiments, the bottom portion of the actuator was hung in the air (27 °C) by several threads to reduce the heat loss through contact with other media. The first experiment was to test the melting time as it related to the current strength and distance between the Ni–Cr wires, which are two vital parameters to adjust the power of the heater. For this experiment, four samples with different wire gaps (1 mm, 1.7 mm, 2.4 mm, and 3.1 mm) were tested. For each sample, four constant currents (0.4 A, 0.5 A, 0.6 A, and 0.7 A) supplied by a DC power unit (MS605D, Maisheng, China) were applied to melt the whole LMPA layer (three trials were conducted for each current). During the heating process, the temperature of the upper surface of the sample was recorded via an infrared camera (Ti400, Fluck Thermography, USA) at an image capture frequency of 9 Hz. Afterward, the videos were analyzed with software (SmartView 4.1, Fluck Thermography, USA) to derive the temperatures at different times. For controlling variable DOF performance, it is better if the temperature boundaries between the liquid and solid sections remain constant. Thus, the other experiment evaluated the collateral effect of heating one section of the LMPA on the adjacent ones. To this end, only the middle section was heated to the melting point with the four currents. The temperature distributions throughout the entire LMPA were obtained by the same method.

To evaluate the cooling speed of the LMPA, we conducted a comparison experiment to test the cooling time of the LMPA in air and water. For air cooling, the LMPA was first heated above the melting point; then the current was suddenly switched off. The temperature change of the bottom surface of the actuator was recorded via the infrared camera. For water cooling, a hydraulic actuation method was used. As figure 2(b) shows, the actuator and two syringes were connected and filled with water. During the test, the actuator was first heated above the melting point; then the active syringe was moved right to put the cold water into the actuator, accelerating the cooling. Meanwhile, the passive syringe was moved left to draw out the hot water in the chamber of the actuator. The temperature change was recorded during the whole process. Two tests were conducted for the water cooling experiment. One was tested using the water at the room temperature (26 °C), while the other using an ice–water mixture.

2.5. Evaluation of the EGaIn sensor

Based on the mathematical model, we use the curvature (which was acquired by the EGaIn sensor) as the key parameter to evaluate the bending of the soft actuator. To calibrate the
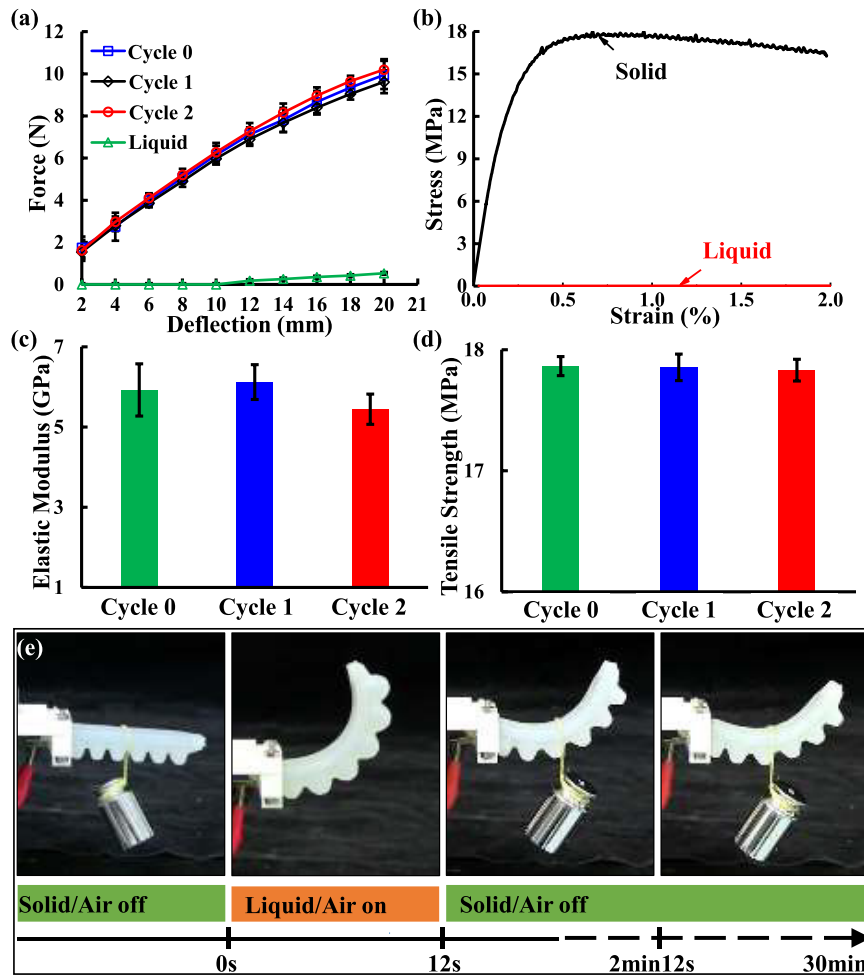
Figure 3. The variable stiffness property of the actuator. (a) The bending force comparison of the actuator between the solid- and liquid-state LMPA. (b) The stress–strain relationship for the solid- and liquid-state LMPA. (c) The elasticity modulus of the actuator under several reheating-recrystallizing cycles. (d) The tensile strength of the actuator under several reheating-recrystallizing cycles. (e) The demonstration of the actuator's shape-maintaining property.

EGaIn sensor for the measurement of the bending curvature, the actuator was fixed to a base, and a constant 30 mA current flowed through the sensor. For each motion pattern, the corresponding LMPA sections were first melted; then the actuator was inflated to a preset pressure for bending. Meanwhile, the voltage variation of the sensor was acquired via an NI data acquisition board (PCI-6284, National Instruments, USA) at the sample rate of 100 Hz. And the final profile of the actuator was captured via a camera. For each motion pattern, seven pressures (8, 12, 16, 20, 24, 27, and 30 kPa) were chosen to inflate the actuator three times. For the details of the calibration process, we inflated the actuator to the preset pressures. Through a constant electrical current provided by the DC power unit (MS605D, Maisheng, China), the resistance variation of the EGaIn sensor between the two electrodes was converted to the voltage values. Then we record the voltage variation of the EGaIn sensor by using a NI data acquisition facility. The bending profile of the soft actuator was captured by a digital camera setup aside simutanously. We obtained the bending curvature of the soft actuator through a Matlab program (Matlab 2014, MathWorks, USA) developed by

ourselves. Through the above process, we obtained the relationship between the bending curvature and the resistance variation map each other one by one at the same pressure. To evaluate the sensitivity of the sensor, we set the actuator to motion pattern 4 then gave a step-input signal by suddenly inflating the actuator to 30 kPa. The pressure and the voltage of the sensor were simultaneously acquired by the data acquisition board with a sample rate of 100 Hz.

3. Results

3.1. Variable stiffness

From figure 3(a), it can be seen that the bending forces of the solid samples increased with the deflection from 2 mm to 20 mm. The bending forces of the samples in the liquid state began to emerge at 10 mm, where the connector contacted the sample, then increased gradually within a very tiny range. Furthermore, the average bending force of all the deflections in the solid state was about 36 times that in the liquid state. Besides the bending force, the tensile stiffness of the actuator
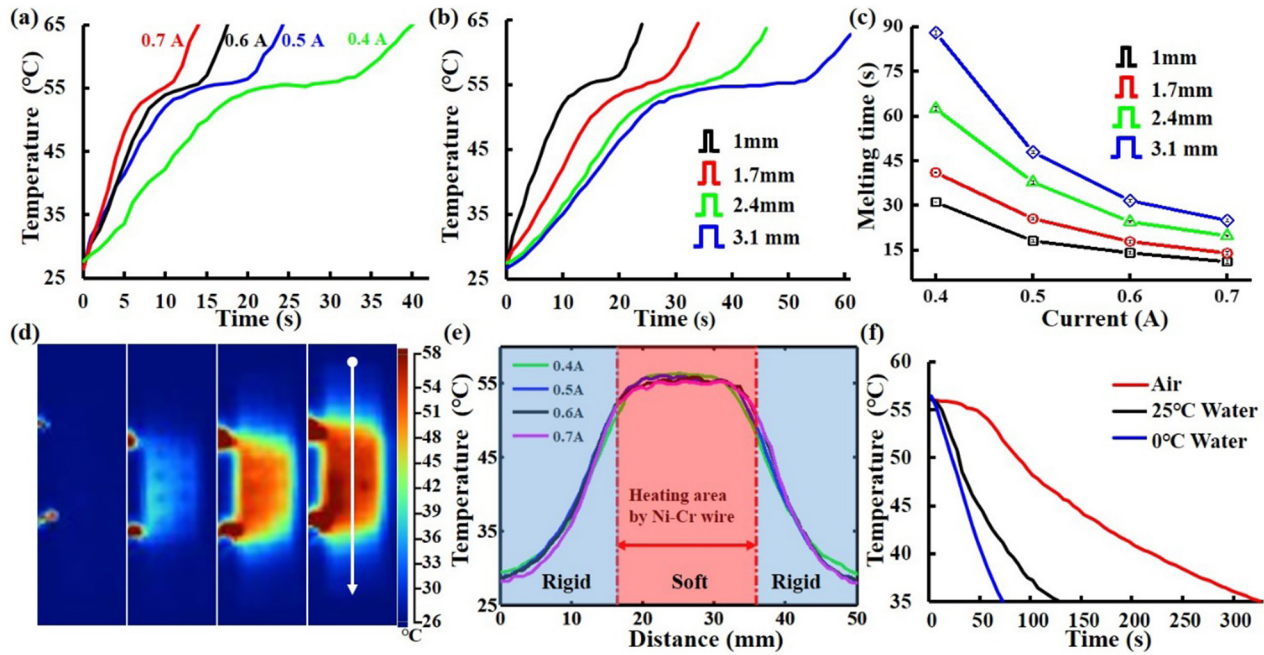
Figure 4. The thermal behavior results of the actuator. (a) The melting process of the LMPA with different currents. The gap between the wires was 1 mm. (b) The melting process of the LMPA with different wire gaps. The current was 0.5 A. (c) The melting time in relation to the currents and wire gaps. The average mass of the LMPA samples was about 3.6 g. (d) The infrared thermal images when only section II of the LMPA was heated with a 0.4 A current. (e) The temperature distribution of the middle line of the LMPA when section II was heated with different currents. The line and the direction were indicated in the last image of the panel (d). The red dashed lines show the position of the heating wire. (f) The cooling time comparison of the LMPA in the open air and with water (and ice–water) actuation.

also increased several magnitudes, which can be verified by figure 3(b). As the results show, the stress in the solid state was much greater than that in the liquid state under the same strain. From figure 3(b) it can also be seen that the elasticity modulus of the sample in the solid state, which was obtained by calculating the slope of the strain–stress curves, is about 4000 times that in the liquid state. It should be noted that the stress in the liquid state was regarded as the force divided by the cross-sectional area of the silicone rubber, while the stress in the solid state was calculated as the force divided by the cross-sectional area of the LMPA layer. The area of the hole was excluded because its size is not negligible compared to that of the whole structure. Furthermore, the mechanical property is also repeatable, which can be verified by figures 3(a), (c) and (d). As the results show, the bending force, elasticity modulus, and tensile strength of the actuator can be maintained throughout several reheating-recrystallizing cycles, which is impossible with other materials such as SMP [22, 36]. Referring to figure 3(e), it can be seen that the actuator can also retain its shape well without power. For the demonstration, we first melted all the sections of the LMPA and inflated the actuator to bend. After the LMPA solidified, which took about 2 min, the pressure was released and the weight hung on the actuator. After 30 min, it was observed that the actuator continued to support the weight despite some slight deformation.

3.2. Melting/solidification speed and temperature distribution

Figure 4 shows the thermal behavior results of the actuator. Referring to both figures 4(a) and (b), the melting process of

the LMPA included three stages. In stage I, the temperature increased to about 55 °C linearly over time, which represented the melting point (this value is below 62 °C because the temperature measured is the surface temperature of the sample). During this stage, the phase of the LMPA was solid. In stage II, the temperature did not change significantly, but the LMPA's state transformed from solid to liquid. In stage III, the LMPA was in a liquid state, and the temperature continued to increase. Figure 4(c) shows the melting time of the LMPA with different currents and wire gaps. Here the melting time was defined as the period during which the LMPA was heated from room temperature to its liquid state. As the results show, the melting time decreased by increasing the current or reducing the wire gap (that is, increasing the resistance of the heater); i.e. increasing the power of the heater. The LMPA could be melted within 12 s with a current of 0.7 A and gap of 1 mm.

Figure 4(d) demonstrates the infrared temperature distribution of the actuator when section II was heated. Figure 4(e) was created by extracting the temperatures of the middle line (the solid white line shown in figure 4(d)) when the LMPA was at its melting point. As the results show, the temperatures have almost the same distribution for all four currents, which may be related to the direction of the heat flow. When powered, most of the generated heat was conducted through the normal section of the surface as the conduction area, and the temperature gradient is much larger than those in the tangential direction. The same distributions with different currents prove that the activated sections have little influence on adjacent ones, which guarantees the repeatability of the DOF after
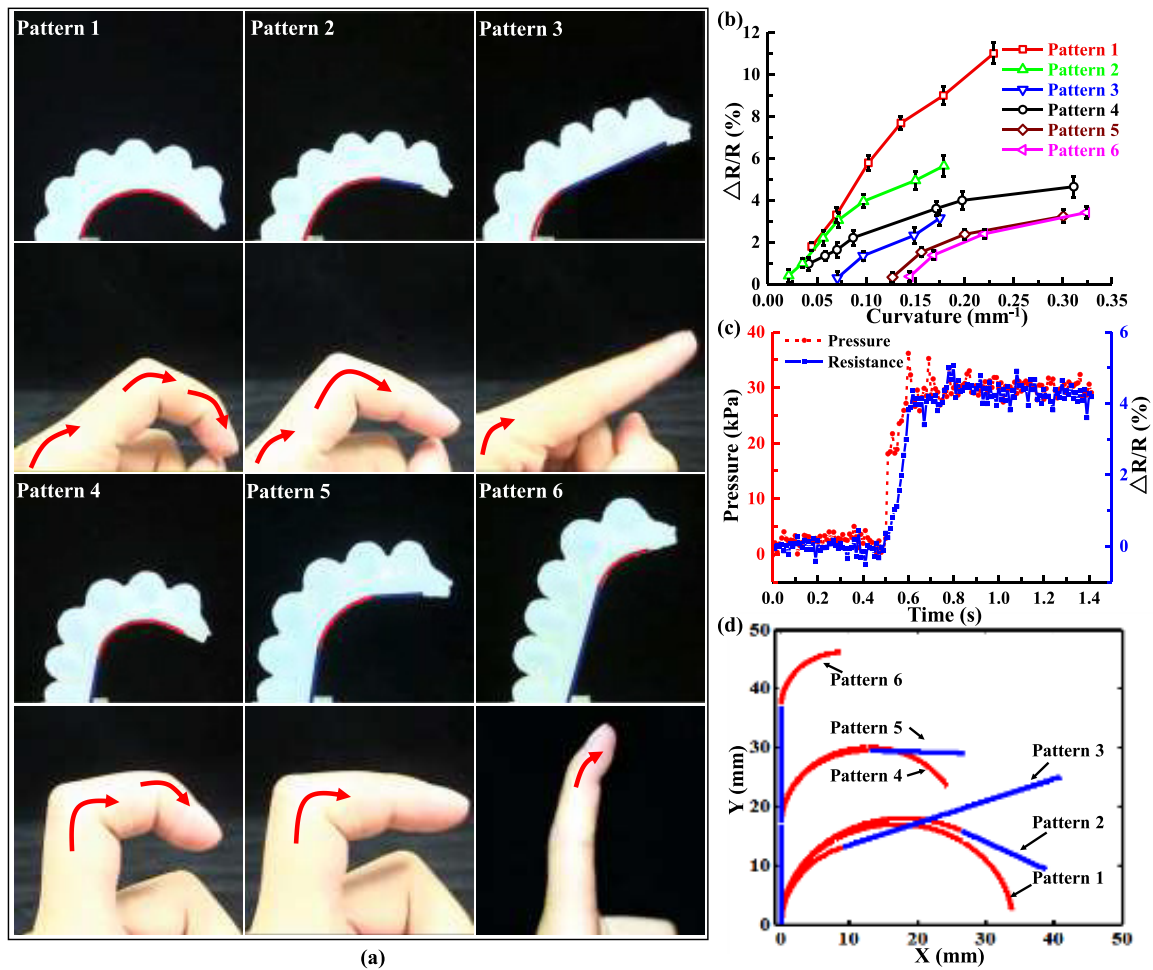
Figure 5. The tunable DOF and sensor feedback results. (a) The various motion patterns of the actuator under the same pressure (30 kPa) and comparison with the index finger of the left hand. The red lines illustrate which sections of the LMPA were liquid, and the blue lines illustrate which were solid. (b) The relationship between the resistance of the sensor and curvature under different motion patterns. (c) The hysteresis test results of the sensor. (d) The results of the sensor-based model for comparing the six motion patterns in panel (a).

several cycles of heating and recrystallizing adjacent sections. Figure 4(f) shows the cooling behavior of the LMPA. As the results show, it took about 325 s for the LMPA to cool from 56 °C to 35 °C in the open air. The time was reduced to 120 s (about 37 % of the time required in open air) if the actuator was actuated by 25 °C water. For the ice–water mixture, the cooling time was cut down to 70 s, about 21 % the time required in the air. The significant differences indicate that water actuation is an excellent way to cut down the cooling time because the specific heat of water is much larger than that of air.

3.3. Tunable DOF and curvature feedback of the soft actuator

Figure 5(a) shows the images of the six motion patterns executed with the same pressure (30 kPa). As the images show, the melted sections can easily bend under actuation, while the bending of the unmelted sections was constrained. Furthermore, it can be seen from figure 5(a) that the actuator can not only mimic all the gestures of an index finger by changing the DOF but can become more flexible than that. The actuator can easily bend joints individually, which is very difficult for

a finger. To demonstrate the tunable DOF, in supplementary video S1 (stacks.iop.org/JMM/28/024004/mmedia) we show all six motion patterns the actuator achieved, compared with an index finger.

Figure 5(b) shows the resistance of the EGaIn sensor in relation to the curvature under different motion patterns. As the results show, the resistance increases with the curvature for all six patterns. For patterns 3, 5 and 6, only four points exist because the resistance varied little when the actuator was deformed to a small degree (with a pressure less than 19 kPa). Furthermore, it can also be seen that the resistances were tiny with a small deformation and resistance increased with more melted sections under the same curvature. This is because the output of the sensor is determined by the deformation of the soft actuator (microchannel). In figure 5(c), we can see that the resistance varied instantly with the step input of the pressure and no hysteresis exists. Thus, the sensor provides feedback about the curvature in real time. To verify the mathematical model, we used the calibrated curvature data as the input, then got the profiles of the actuator for the six motion patterns shown in figure 5(a). As figure 5(d) shows, the sensor-based model can reconstruct the approximate position
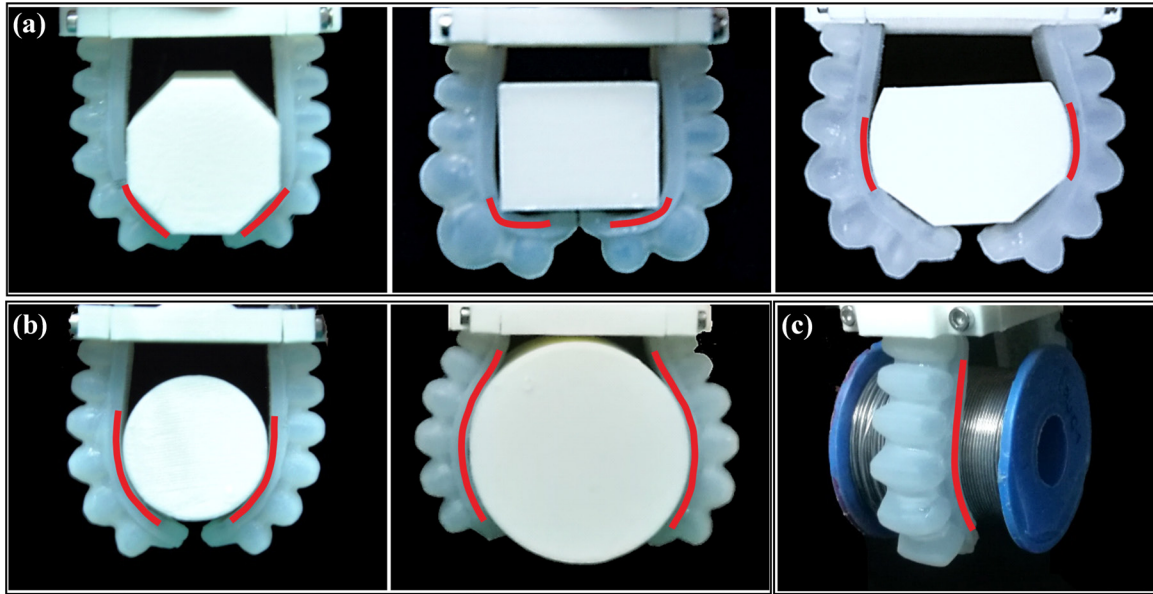
Figure 6. Demonstration of the gripper's grasping ability. (a) The gripper can grasp objects with different shapes by changing its motion patterns. (b) The gripper can grasp objects with different sizes by changing its bending length. (c) The gripper can grasp an object of around 280 g, 20 times the weight of a single actuator. The red lines indicate heated sections of the LMPA layer.

of the actuator. Some inconsistencies exist because the base of the actuator was bent by the inflated chamber, which could be solved by improving the structure.

3.4. The grasping demonstration

Figure 6 demonstrates the grasping performance of the gripper. As figure 6(a) shows, the gripper can properly contact different contours by selecting different motion patterns for the actuator, which would be impossible if the actuator had only one bending section. Furthermore, the grasping space can be adjusted by selecting the bending length of the actuator, so the gripper can fully adapt to the objects of different sizes (as figure 6(b) shows). Besides the tunable DOF, the stiffness enhancement guarantees that the gripper can grasp heavy objects. As figure 6(c) shows, the gripper can grasp a solder coil with the weight of 280 g, which is about 20 times that of a single actuator. It should be noted that the load capacity was limited by the bending of the actuator. Supplementary video S2 demonstrates the grasping performance when gripping these items.

4. Discussion

Recent studies on variable stiffness of soft robotics have encountered various challenges. Particle jamming [8, 9] needs a high volume to increase stiffness and external auxiliary devices such as pumps and valves to adjust the pressure. Smart fluids [10, 11] depend on complicated devices to regulate magnetic or electric fields. SMP [13] has a poor thermal conductivity that leads to slow response times. SMA [15] has high absolute rest stiffness that prevents their application in soft robots. In this paper, we chose LMPA as the embedded material because the stiffness range it can alter is much wider than most other materials (as the results in figures 3(a) and

(b) show). LMPA phase transformation can be achieved by Joule heating, which requires a very simple control system. Furthermore, the mechanical properties of the material can be restored from a damaged state by the reheating-recrystallization method, verified by figures 3(a), (c) and (d).

Although soft robots' motion can be manipulated by attaching fibers [18], sleeves [20], or fabric patches [21] to different portions of the actuators, the motion patterns are pre-programmed and cannot be changed after fabrication. To change the DOF during operation, some studies have embedded SMP at the arthroses of the actuator [22]. However, the maximum stiffness is still limited compared to that achieved with LMPA. Additionally, shape memory actuators cannot retain their positions without power input. By selectively melting different sections of the LMPA, the DOF of the present study's actuator could also be changed during operation (as figure 5(a) shows). The actuator can maintain its shape with zero energy consumption (shown in figure 4(e)) when the LMPA layer is solidified (at the rigid state).

Although the LMPA could also be melted by direct Joule heating [24] because it is conductive. However, the structure will be limited to the series-wound shape based on the current flows; also, the circuit will be interrupted if the structure is broken. Some previous work also applied liquid metal sealed in the microchannel as the heater [37]. However, the power of the heater is limited by the dimension of the microchannel, which is difficult to fabricate on an extremely small scale. In our study, the commercial Ni–Cr wire was chosen because its electrical resistivity is about 62.3 times that of copper. The diameter of the wire is only 100 μm, therefore, the Ni–Cr wires have minimal influence on the mechanical property of the actuator. The Ni–Cr wire is a simple but very robust and efficient method for heating [38].

According to our results, the LMPA could be melted within 12 s to complete the solid–liquid phase transition. The stiffness of the LMPA changes significantly when it reaches the

melting point. It should be noted that, the melting time can be further shortened by a preheating process. For example, as figure 4(c) shows, it takes less than 5 s to heat the LMPA from 40 °C to its melting point. In the future, accelerating the melting process with preheating treatment would complement our current design.

In figure 4(d) we can see that pumping cold water into the chamber of the soft actuator can accelerate the cooling/solidification of the LMPA. For fast melting/cooling, we believe that hydraulic actuation, with the ability to preheat/cool the LMPA, is promising. This can be achieved by adding a heater into one of the syringes shown in figure 2(b). During the heating process, the syringe with the heater could inject hot water into the chamber of the actuator for preheating. For cooling, the hot water could be drawn out, and cold water could be pumped into the chamber.

To enhance the EGaIn sensor's resolution, we placed the microchannel on a location of the soft actuator where maximum strain is produced during bending. For further improvement in the future, channel with smaller cross section will be fabricated using high-precision equipment such as micro laser machining. For reliable grasping, the compliance of the gripper and its adaptability to the contour of the objects are essential. Traditional soft grippers' actuators can only produce profiles with constant curvatures [1, 34]. Although the articulated soft gripper can control its stiffness and bending position, the contact between the gripper and the object is not complete either because only its joints may bend [22]. In contrast, the gripper proposed in our research can actively adapt to fully grip another surface because of two advantages (as shown in figure 6): (1) we can program a desired DOF according to the shape and size of the gripped object, and (2) the activated sections can bend completely to maintain full contact with the contours of gripped objects.

5. Conclusion

In this study, we presented a soft actuator, embedded with two kinds of eutectic metals, with variable stiffness, tunable DOF, and sensing properties. To achieve variable stiffness and tunable DOF, LMPA, whose different sections could be melted via Ni–Cr wires beneath it, was embedded in the bottom of the actuator. For positional feedback, EGaIn was injected into the microchannel of the actuator. Systematic thermal conduction experiments revealed that the LMPA could be melted within 12 s. And the crystallization time of the LMPA could be reduced to 70 s when actuated with ice–water mixture. What's more, the heater could guarantee the repeatability of the variable DOF. The mechanical experiments demonstrated that the bending strength and tensile strength of the actuator both significantly improved when the LMPA was in its solid state. The sensor-based mathematical model revealed that it could measure the approximate position of the actuator under larger deformation. Finally, the two-fingered gripper demonstrated the superiority of changing the DOF. Based on the geometric configurations of different objects, the gripper can alter its grasping strategies by changing its DOF. Thus, the gripper can grip target objects of different sizes and shapes.

To further improve the capability of the actuator, we are fabricating a hydraulic system that pumps hot water to preheat the LMPA and uses cold water to accelerate crystallization. Additionally, we will also test new fabrication methods to reduce the size of the microchannel to improve the sensitivity of the EGaIn sensor, as well as using fabrication approach such as multi-material 3D printing technology to implement the soft actuator [39, 40].

ORCID iDs

Li Wen ⓘ https://orcid.org/0000-0002-1498-3103

References

[1] Hao Y, Gong Z, Xie Z, Guan S, Yang X, Ren Z, Wang T and Wen L 2016 Universal soft pneumatic robotic gripper with variable effective length *2016 35th Chinese Control Conf. (Chengdu, China)* (IEEE) pp 6109–14

[2] Wehner M, Truby R L, Fitzgerald D J, Mosadegh B, Whitesides G M, Lewis J and Wood R J 2016 An integrated design and fabrication strategy for entirely soft, autonomous robots *Nature* **536** 451–5

[3] Wang Y *et al* 2017 A biorobotic adhesive disc for underwater hitchhiking inspired by the remora suckerfish *Sci. Robot.* **2** eaan8072

[4] Park Y L, Chen B R, Pérez-Arancibia N O, Young D, Stirling L, Wood R J, Goldfield E C and Nagpal R 2014 Design and control of a bio-inspired soft wearable robotic device for ankle–foot rehabilitation *Bioinspiration Biomim.* **9** 016007

[5] Ranzani T, Gerboni G, Cianchetti M and Menciassi A 2015 A bioinspired soft manipulator for minimally invasive surgery *Bioinspiration Biomim.* **10** 035008

[6] Stilli A, Grattarola L, Feldmann H, Wurdemann H A and Althoefer K 2017 Variable stiffness link (VSL): toward inherently safe robotic manipulators *2017 IEEE Int. Conf. on Robotics and Automation (ICRA) (Singapore)* (IEEE) pp 4971–6

[7] Jusufi A, Vogt D M, Wood R J and Lauder G V 2017 Undulatory swimming performance and body stiffness modulation in a soft robotic fish-inspired physical model *Soft Robot.* **4** 202–10

[8] Wei Y, Chen Y, Ren T, Chen Q, Yan C, Yang Y and Li Y 2016 A novel, variable stiffness robotic gripper based on integrated soft actuating and particle jamming *Soft Robot.* **3** 134–43

[9] Wall V, Deimel R and Brock O 2015 Selective stiffening of soft actuators based on jamming *2015 IEEE Int. Conf. on Robotics and Automation (ICRA) (Seattle, USA)* (IEEE) pp 252–7

[10] Majidi C and Wood R J 2010 Tunable elastic stiffness with microconfined magnetorheological domains at low magnetic field *Appl. Phys. Lett.* **97** 164104

[11] Sadeghi A, Beccai L and Mazzolai B 2012 Innovative soft robots based on electro-rheological fluids *2012 IEEE/RSJ Int. Conf. on Intelligent Robots and Systems (IROS) (Vilamoura, Portugal)* (IEEE) pp 4237–42

[12] Yuen M C, Bilodeau R A and Kramer R K 2016 Active variable stiffness fibers for multifunctional robotic fabrics *IEEE Robot. Autom. Lett.* **1** 708–15

[13] Firouzeh A, Salerno M and Paik J 2015 Soft pneumatic actuator with adjustable stiffness layers for multi-dof actuation *2015 IEEE/RSJ Int. Conf. on Intelligent Robots and Systems (IROS) (Hamburg, Germany)* (IEEE) pp 1117–24

[14] Shan W, Diller S, Tutcuoglu A and Majidi C 2015 Rigidity-tuning conductive elastomer *Smart Mater. Struct.* **24** 065001

[15] Li J, Zhong G, Yin H, He M, Tan Y and Li Z 2017 Position control of a robot finger with variable stiffness actuated by shape memory alloy *2017 IEEE Int. Conf. on Robotics and Automation (ICRA)2017 (Singapore)* (IEEE) pp 4941–6

[16] Martinez R V, Branch J L, Fish C R, Jin L, Shepherd R F, Nunes R, Suo Z and Whitesides G M 2013 Robotic tentacles with three-dimensional mobility based on flexible elastomers *Adv. Mater.* **25** 205–12

[17] Drotman D, Jadhav S, Karimi M and Tolley M T 2017 3D printed soft actuators for a legged robot capable of navigating unstructured terrain *2017 IEEE Int. Conf. on Robotics and Automation (ICRA) (Singapore)* (IEEE) pp 5532–8

[18] Connolly F, Polygerinos P, Walsh C J and Bertoldi K 2015 Mechanical programming of soft actuators by varying fiber angle *Soft Robot.* **2** 26–32

[19] Martinez R V, Fish C R, Chen X and Whitesides G M 2012 Elastomeric origami: programmable paper-elastomer composites as pneumatic actuators *Adv. Funct. Mater.* **22** 1376–84

[20] Galloway K C, Polygerinos P, Walsh C J and Wood R J 2013 Mechanically programmable bend radius for fiber-reinforced soft actuators *2013 16th Int. Conf. on Advanced Robotics (ICAR) (Montevideo, Uruguay)* (IEEE) pp 1–6

[21] Sun Y, Yap H K, Liang X, Guo J, Qi P, Ang M H Jr and Yeow C H 2017 Stiffness customization and patterning for property modulation of silicone-based soft pneumatic actuators *Soft Robot.* **4** 251–60

[22] Yang Y, Chen Y, Li Y, Chen M Z and Wei Y 2017 Bioinspired robotic fingers based on pneumatic actuator and 3D printing of smart material *Soft Robot.* **4** 147–62

[23] Mohammadi Nasab A, Sabzehzar A, Tatari M, Majidi C and Shan W 2017 A soft gripper with rigidity tunable elastomer strips as ligaments *Soft Robot.* (https://doi.org/10.1089/soro.2016.0039)

[24] Schubert B E and Floreano D 2013 Variable stiffness material based on rigid low-melting-point-alloy microstructures embedded in soft poly (dimethylsiloxane) (PDMS) *RSC Adv.* **3** 24671–9

[25] Van Meerbeek I M, Mac Murray B C, Kim J W, Robinson S S, Zou P X, Silberstein M N and Shepherd R F 2016 Morphing metal and elastomer bicontinuous foams for reversible stiffness, shape memory, and self-healing soft machines *Adv. Mater.* **28** 2801–6

[26] Zhao R, Yao Y and Luo Y 2016 Development of a variable stiffness over tube based on low-melting-point-alloy for endoscopic surgery *J. Med. Devices* **10** 021002

[27] Tonazzini A, Mintchev S, Schubert B, Mazzolai B, Shintake J and Floreano D 2016 Variable stiffness fiber with self-healing capability *Adv. Mater.* **28** 10142–8

[28] Park Y L, Chen B R and Wood R J 2012 Design and fabrication of soft artificial skin using embedded microchannels and liquid conductors *IEEE Sens. J.* **12** 2711–8

[29] Boley J W, White E L, Chiu G T C and Kramer R K 2014 Direct writing of gallium-indium alloy for stretchable electronics *Adv. Funct. Mater.* **24** 3501–7

[30] Majidi C, Kramer R and Wood R J 2011 A non-differential elastomer curvature sensor for softer-than-skin electronics *Smart Mater. Struct.* **20** 105017

[31] Tiziani L O, Cahoon T W and Hammond F L 2017 Sensorized pneumatic muscle for force and stiffness control *2017 IEEE Int. Conf. on Robotics and Automation (ICRA) (Singapore)* (IEEE) pp 5545–52

[32] Bilodeau R A, White E L and Kramer R K 2015 Monolithic fabrication of sensors and actuators in a soft robotic gripper *2015 IEEE/RSJ Int. Conf. on Intelligent Robots and Systems (IROS) (Hamburg, Germany)* (IEEE) pp 2324–9

[33] Mosadegh B, Polygerinos P, Keplinger C, Wennstedt S, Shepherd R F, Gupta U, Shim J, Bertoldi K, Walsh C J and Whitesides G M 2014 Pneumatic networks for soft robotics that actuate rapidly *Adv. Funct. Mater.* **24** 2163–70

[34] Wakimoto S, Suzumori K and Ogura K 2011 Miniature pneumatic curling rubber actuator generating bidirectional motion with one air-supply tube *Adv. Robot.* **25** 1311–30

[35] Manti M, Hassan T, Passetti G, D'Elia N, Laschi C and Cianchetti M 2015 A bioinspired soft robotic gripper for adaptable and effective grasping *Soft Robot.* **2** 107–16

[36] Yang Y, Chen Y, Li Y, Wang Z and Li Y 2017 Novel variable-stiffness robotic fingers with built-in position feedback *Soft Robot.* (https://doi.org/10.1089/soro.2016.0060)

[37] Shan W, Lu T and Majidi C 2013 Soft-matter composites with electrically tunable elastic rigidity *Smart Mater. Struct.* **22** 085005

[38] Hao Y, Wang T and Wen L 2017 A programmable mechanical freedom and variable stiffness soft actuator with low melting point alloy *The Int. Conf. on Intelligent Robotics and Applications* pp 151–61

[39] Wen L, Weaver J and Lauder G 2014 Biomimetic shark skin: design, fabrication and hydrodynamic function *J. Exp. Biol.* **217** 1656–66

[40] Wen L, Weaver J, Thornycroft P and Lauder G 2015 Hydrodynamic function of biomimetic shark skin: effect of denticle pattern and spacing *Bioinspiration Biomim.* **10** 066010